

## The effect of annealing temperature on the optical properties of aluminum-doped zinc oxide nanostructures

Abass Raheem Soodi<sup>\*1</sup>, Hayder.J.Al-Asedy<sup>1</sup>

<sup>1</sup>Physics Department, Faculty of Education, University of Al-Qadisiyah,  
Diwaniyah, Iraq

\*Corresponding Author E-mail: [edu-phy10.post@qu.edu.iq](mailto:edu-phy10.post@qu.edu.iq)

### ARTICLE INF.

#### Article history:

Received: 23 MAY., 2024

Revised: 2 AUG., 2024

Accepted: 2 AUG., 2024

Available Online: 29 DEC.  
2024

#### Keywords:

Annealing temperature;  
glass substrate;  
spin coating;  
optical properties; AZO  
nanostructures.

### ABSTRACT

The AZO nanostructure samples used in this investigation were made on a glass substrate by spin-coating utilizing an inexpensive sol-gel method. We investigated the effects of annealing temperature on AZO (aluminum doped with zinc) thin film on optical characteristics. The films were annealed in an air environment at (350, 400, 450, 500, and 550) °C for four hours. The measurements of optical transmittance and absorbance were made in the 300–800 nm wavelength range using a single beam spectrophotometer. When the temperature of annealing increases, the optical band gap decreases from 3.36 eV to 3.2 eV and the UV–Vis absorption spectra exhibit a small red shift. The AZO films have transmittances over 35% in the IR region of spectrum for 350°C after annealing sample, but rises to 95% at 550°C after annealing at higher temperatures. With a rise in annealing temperature, AZO film extinction coefficient increased. An increase in annealing temperature results in an increase in both optical and electrical conductivities. The AZO films were characterized with respect to their optical properties using UV-vis spectroscopy, and the optical band gap was computed using the Tauc method. The optical test indicated a direct nature of the optical transition, with an average band gap energy propensity to decrease from 3.36 to 3.20 eV when the temperature was elevated from 350 to 550 °C during the temperature annealing process. The experimental results indicate that the properties of the AZO films were affected by the annealing.

DOI: <https://doi.org/10.31257/2018/JKP/2024/v16.i02.16316>

تأثير درجة حرارة التلدين على الخواص البصرية للبنى النانوية لأكسيد الزنك المضاف إليه الألمنيوم

عباس رحيم سودي<sup>1</sup>، حيدر جواد مكطوف<sup>\*1</sup>

<sup>1</sup>قسم الفيزياء، كلية التربية، جامعة القادسية، الديوانية، العراق

الكلمات المفتاحية:

الخلاصة

درجة حرارة التلدين؛ ركيزة زجاجية؛  
الطلاء الدوراني؛ الخصائص  
البصرية؛ تراكيب أوكسيد الخارصين  
المشوب بالألمنيوم النانوية.

تم تصنيع عينات البنية النانوية لـ AZO المستخدمة في هذا البحث على ركيزة زجاجية عن طريق الطلاء الدوراني باستخدام طريقة المحلول-الهلامي الرخيصة. لقد بحثنا في تأثيرات تغير درجة حرارة التلدين على طبقة AZO الرقيقة (الألمنيوم المشوب بأوكسيد الزنك) على الخصائص البصرية حيث تم تلدين الأغشية في بيئة الهواء الجوي عند (350 و 400 و 450 و 500 و 550) درجة مئوية لمدة أربع ساعات. تم إجراء قياسات النفاذية والامتصاص الضوئي في نطاق الطول الموجي (300-800) نانومتر باستخدام مطياف شعاع واحد. عندما ترتفع درجة حرارة التلدين، تقل فجوة النطاق الضوئي من 3.36 إلكترون فولت إلى 3.2 إلكترون فولت وتظهر أطراف امتصاص الأشعة فوق البنفسجية والمرئية انزياحاً أحمر صغيراً. تتميز أغشية AZO بنفاذية تزيد عن 35% في منطقة الأشعة تحت الحمراء التي تشع هذا الطيف عند 350 درجة مئوية بعد التلدين، ولكنها ترتفع إلى 95% عند 550 درجة مئوية بعد التلدين عند درجات حرارة أعلى. مع ارتفاع درجة حرارة التلدين، زاد معامل الخمود فيلم AZO؛ تؤدي زيادة درجة حرارة التلدين إلى زيادة في كل من الموصلية الضوئية والكهربائية. تم تمييز أفلام AZO فيما يتعلق بخصائصها الضوئية. باستخدام مطيافية الأشعة فوق البنفسجية المرئية، وتم حساب فجوة النطاق الضوئي باستخدام طريقة Tauc. أشارت الخصائص البصرية إلى طبيعة مباشرة للانتقال الضوئي، مع ميل متوسط طاقة فجوة النطاق إلى الانخفاض من 3.36 إلى 3.20 إلكترون فولت عند رفع درجة الحرارة من 350 إلى 550 درجة مئوية أثناء عملية التلدين الحراري. تشير النتائج التجريبية إلى أن خصائص أفلام AZO تأثرت بالتلدين الحراري.

## 1. INTRODUCTION

The number of ZnO related papers has expanded steadily over the past ten years, and as of 2007, it was Silicon's closest competitor as the most widely used semiconductor. The ZnO has a number of advantageous qualities, including intense luminescence, wide and straight band gap, and high electron mobility [1]. As a result, it has attracted great attention of semiconductor researches. These characteristics are already utilized in cutting-edge uses for thin-film transistor and light-emitting diode applications in electronics, solar cells, sensors, and detectors; transparent electrodes in liquid crystal displays; heat-resistant, energy-efficient windows [2]. Modern solar cell, sensor, and detector applications; transparent electrodes in liquid crystal displays; and heat-resistant, energy-efficient windows are already using these properties; and thin-film transistor and light-emitting diode applications in electronics. Several deposition processes have been used to generate ZnO thin films, including sputtering [3], molecular beam epitaxy [4], spray pyrolysis [6], pulsed laser deposition

[5], and the sol-gel deposition process [7]. The sol-gel deposition process is not only easier to use, but it also provides the opportunity to prepare a large-area deposition at a low cost and at a relatively low temperature. As previously documented, sol-gel process variables including precursor concentration and aging time frequently affect the properties of the films [8]. Studies have also been done on the impact of annealing temperature [9]. However, annealing temperatures exceeding 400 °C were the main focus of the majority of the studies. Sengupta et al. [10], for instance, evaluated the impact at annealing temperatures between 400 and 700 °C, depending on the optical and structural characteristics of ZnO films. Because glass and plastic substrates can only withstand temperatures of 500 °C, this temperature limit may be an issue. Determining the ideal annealing temperature for AZO film production on glass substrates necessitates looking at the impacts of a lower temperature annealing procedure. In this work, the sol-gel spin coating process was used to produce AZO films onto a glass substrate. The primary aims of this

study are to determine the optimal annealing temperature and to assess how annealing temperatures in the low range (350–550 °C) affect the optical properties and quality of AZO films.

## 2. EXPERIMENTAL

### 2.1 Glass-substrate cleaning:

The ZNFs were created utilizing the sol-gel allied spin coating method using glass substrates measuring 2.5 cm by 2.5 c. Initially, Decon 90 surfactant solutions were used to rinse these substrates for 15 minutes in order to remove any impurities that had become adhered to the surface. To remove the ions that were on the surface, these substrates were then cleaned in deionized water. It is well known that impurities on the surface layer frequently cause the deposited film to adhere poorly, which results in pinholes on the film's surface. Following the cleaning processes, these substrates were oven dried for 25 minutes at 150 °C in order to remove any last traces of solvent or water from the surface.

### 2.2 Precursor solution preparation:

The AZNFs were deposited using ethanolamine (Alfa Aesar), 2-propanol, and highly pure (99.999%) zinc acetate dehydrates, or ZAD. To dissolve ZAD (0.1M),  $\text{Al}(\text{NO}_3)_3 \cdot 9\text{H}_2\text{O}$ , aluminum nitrate nonahydrate, was added to the mixture, 2-propanol and ethanolamine were first produced as a solution at ambient temperature. The ethanolamine and ZAD had a 1:1 molar ratio. After that, the liquid was magnetically agitated for 30 minutes to produce a clear, homogenous solution. By obtaining the NFs, the resultant mixture (a few drops) was then applied on the glass substrate. This was

followed by spin coating for roughly 30 seconds at a speed of 3000 rpm. For each sample, the identical procedure was carried out ten times in order to produce a consistent AZNSs. Lastly, the spin-coated film was dried for around 20 min at 220 °C in an electrical oven.

## 3. RESULTS AND DISCUSSION

### 3.1. Absorbance Spectra:

Figure 1 illustrates the typical UV/visible absorption coefficient of produced AZO NSs for the five samples at temperatures used for annealing (350, 400, 450, 500, and 550) °C with fixed annealing time 4.00 hr. Since every sample has a distinct absorption edge, all of the films were of high quality.

A single beam spectrophotometer was used to test the optical transmittance and absorbance at ambient temperature in the 300–800 nm wavelength range. According to this figure, the absorption coefficient spectrum shows that light was absorbed more in the ultraviolet region and much less in the visible zone. Using the connection, the absorption coefficient [11] was calculated (1):

$$\alpha = 2.303 \frac{A}{t} \dots\dots\dots(1)$$

where  $a$  is the absorbance,  $t$  is the thickness, and  $\alpha$  is the absorption coefficient. The annealing temperature of an AZO thin film causes a little movement of the absorption edge in the direction of the longer wavelength. This suggests that the optical absorption edge has slightly shifted red, which could be related to the annealing temperature increasing and causing an increase in AZO grain size. This provides information about the

excitonic and inter transition nanostructures [12].

The spectra demonstrate that the nanostructure samples exhibit strong UV absorption at range (300-350) nm and low absorption in the visible light (400-700) nm and fixed absorption at near and far infrared areas. While the absorption edge moving to the lower energy refers to some local energy levels generated by some intrinsic defects, the optical absorption at the

absorption edge correlates the change in phase from the valence band to the conduction band [13]. Our results were entirely compatible with the researcher's findings, which indicates that for all AZO samples, the absorbance maxima were brought about by electron shifts inside the valence band (O2p-Zn3d) below 400 nm, to the intrinsic band gap absorption of the conduction band [14].

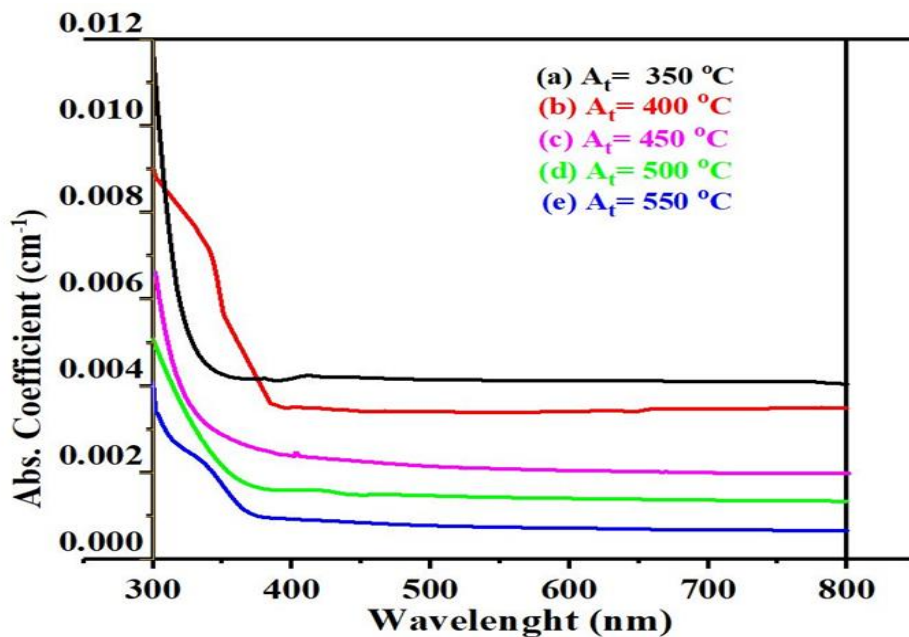


Figure 1. Absorption Coefficient for various annealing temperatures as a function of wavelength, (a) 350 °C, (b) 400 °C, (c) 450 °C, (d) 500 °C and (e) 550 °C

### 3.2. The Skin depth:

The skin depth, also known as penetration depth, is a measure of how electromagnetic waves degrade as they enter conducting medium. The current of photons density peaks at the surface and then exponentially declines from there, throughout the semiconductor. This decline is caused by many factors, including microstructure, refractive index, and surface morphology. Skin depth is also influenced by frequency,

optical conductivity, and photons, which the optical photon density drops to 37% or (1/e), of its original value. The term skin depth ( $\Phi$ ) refers to the surface. It indicates the depth to which a conductor can be penetrated by an electric field, magnetic field, or current. In other words, the penetration depth, which measures the extent to which light or any other electromagnetic radiation may enter a material, is the depth at which the intensity of the

radiation inside the material decreases to this value of its initial value. The following relationship (2) indicates that the optimal parameter for estimating penetration depth is the absorption coefficient [15].

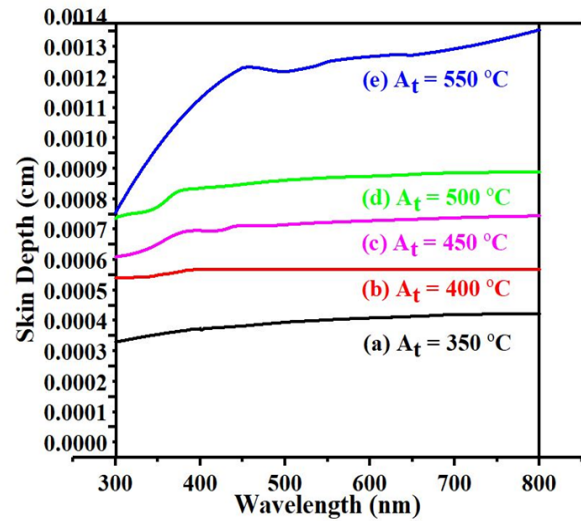
$$\Phi = \frac{1}{\alpha} \dots\dots\dots(2)$$

Fig. (2) shows how the predicted skin depth ( $\Phi$ ) increases with the wavelength increased for the one AZO NSs sample, and also with increased annealing temperature the skin depth increased because the decreasing in absorption coefficient ( $\alpha$ ) with the wavelength for the generated AZO NSs. This Figure allows one to draw the following conclusions:

- a- When the wavelength is near the ( $\lambda_{cut-off}$ ), there is a significant likelihood of absorption and a short distance inside the film thickness that reduces the incident photon amplitude by a factor of (e), resulting in a small skin depth.
- b- The absorption effect disappears and the amplitude decreases after traveling a greater distance at wavelengths greater than the ( $\lambda_{cut-off}$ ) inside the visible area, meaning that the skin depth will be significant.

From the Figure below it is clear, as previously indicated, the irregular surface of the AZO film may be the cause of the peak oscillation in the curve. Figure 2 indicates that as the annealing temperature rose, the skin depth dropped and the visible area of the spectrum expanded while the UV section shrank, this is because the electromagnetic wave will be traveling at a very thick film before losing

amplitude. Our results were contrary to the researcher's results [16].



**Figure 2: Skin depth for various annealing temperatures as a function of wavelength: (a) 350 °C, (b) 400 °C, (c) 450 °C, (d) 500 °C and (e) 550 °C**

**3.3 The Optical Band Gap Energy:**

The optical energy of the band gap of the films  $E_g$  was calculated using the  $h\omega$  in the x-axis and the intercept of the linear component of each curve at various annealing temperatures. The band gap of bulk ZnO (3.37 eV) and the calculated band gap energy  $E_g$  value were nearly the same. As shown in Figure. 3, the values of band gap energy can be derived by locating the intercept on the energy axis  $(\alpha h\nu)^2 = 0$  and extrapolating the linear component of the curves.

For the band gap, as the annealing temperature rises from 350 to 550 °C, the value is seen to fall from 3.36 to 3.20 eV. This could be explained by the films' decreased flaws and greater crystallinity at higher annealing temperatures decrease in the optical band gap with increasing annealing

temperature. Similar findings were documented in the research by [17]. Next, the optical band gap for a direct band semiconductor was computed using the following formula [18]:

$$\alpha h\nu = A (h\nu - E_g)^n \quad \dots\dots(3)$$

where A is a constant,  $h\nu$  is the photon energy, and  $E_g$  is the optical band gap.

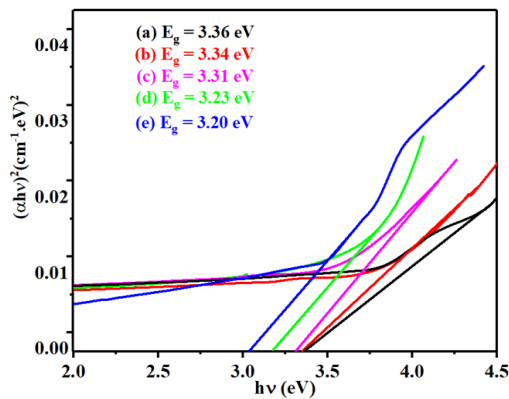


Figure 3 shows the optical band gap energy at 350 °C, 400 °C, 450 °C, 500 °C, and 550 °C for each of the annealing temperatures.

The AZO thin films' large band gap value makes them potential candidates for window or buffer layers in thin-film solar cells. The undoped ZnO film's optical band gap (3.37 eV) is somewhat more than the AZO films'. The red shift of the AZO films in this case was happened because of decreasing in the defects of these films, and vice versa and generally the blue shift of absorption edge in these films are linked to a rise in carrier concentration, which prevent the lowest conduction band states a phenomenon widely referred to as the Burstein-Moss effect [19]. Our findings were entirely in line with the researcher's findings [19].

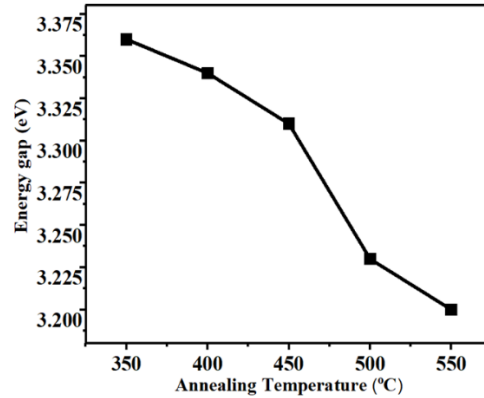


Figure 4: AZO films' optical band gap at various annealing temperatures

As can be seen from Figure 4, the enhanced crystallinity and reduced imperfections together with the optical band gap reduction with increased annealing temperature may be due to the films with higher annealing temperatures.

### 3.4. Extinction Coefficient (K):

The extinction coefficient fluctuation of thin AZO films for different annealing temperatures with (350, 400, 450, 500 and 550)°C in the wavelength range (300–800) nm is shown in Figure (5), this Figure makes it abundantly evident that the extinction coefficient rises with decreasing wavelength and is lowest in the visible wavelength region, for the first four samples except the sample annealed with (550) °C, the behavior of the last can be seen rises after the beginning the visible light (after 400 nm) with increasing wavelength. The high coefficient of absorption may be the cause of the extinction coefficient's behavior. Extinction is highest at the longer wavelengths. This pattern of extinction coefficient can be explained by a higher absorption coefficient. The

longest wavelengths exhibit the largest levels of extinction.

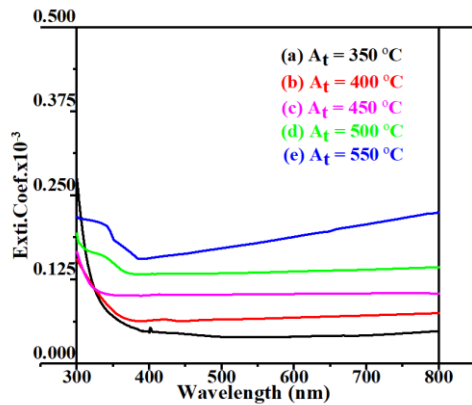


**Figure 5 shows the extinction coefficient for each of the following temperatures for annealing: 350, 400, 450, 500 and 550 °C**

As light travels through the substance, it is absorbed, and defined by the extinction coefficient or (K). Figure 5 demonstrates how the extinction coefficient's behavior resembles the absorption coefficient's curve due to the mentioned relationship [20].

$$K = \frac{\alpha\lambda}{4\pi} \dots \dots \dots (4)$$

Where K represents the extinction coefficient. It increased as the annealing temperature rose, although it had a slightly steep edge that brought it close to absorption. The Sellmeier connection for extinction coefficient and the extinction coefficient's dispersion trend were in agreement. The K decreased with thickness as a result of an increase in the intrinsic free carrier density in the conduction band. Growing the absorption could be the cause of these results. Our findings entirely agreed with the researcher's findings [21].

**3.5. The Optical Conductivity ( $\sigma_{opt.}$ ):**

The optical conductivity of the Al doped ZnO NSs was also estimated using equation (5).

$$\sigma_{opt.} = \frac{\alpha n c}{4\pi} \dots \dots \dots (5)$$

where the absorption coefficient, refractive index, and light speed, respectively, are represented by  $\alpha$ ,  $n$ , and  $c$ .

The change in optical conductivity ( $\sigma_{opt.}$ ) with varying annealing temperatures as a function of wavelength explained in Figure (6), this figure shows that as the annealing temperature rises, the optical conductivity value decreases somewhat in the high wavelength region, or in the visible light spectrum, but drops dramatically in the low wavelength (near the absorption edge). This indicates that the absorption coefficient, bandgap energy ( $E_g$ ), and refractive index ( $n$ ) are all proportional to this value.

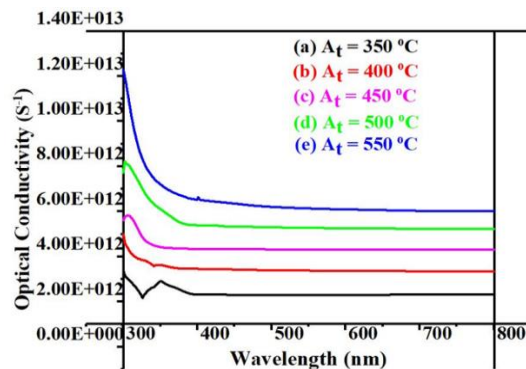


**Figure 6 shows the optical conductivity for each of the following annealing temperatures: 400, 500, 450, 350 and 550 °C**

Furthermore, these high optical conductivity values of the produced AZO nanosheets indicated the material's superiority for these kinds of solar applications [11]. The outcomes were comparable to what was found by [23]. Since  $\sigma_{opt}$  depends on the imaginary part of the dielectric

constant, variations in optical conductivity differ from variations in the imaginary component.

**3.6. The Electrical Conductivity ( $\sigma_{ele.}$ ):**

The relationship between the electrical conductivity [24] of AZO sheets and the optical conductivity  $\sigma_{opt}$  and absorption coefficient  $\alpha$  may be found (6).

$$\sigma_{ele.} = \frac{2\lambda\sigma_{opt.}}{\alpha} \dots\dots(6)$$

Figure 7 represents the relationship between electrical conductivity  $\sigma_{Ele.}$  and wavelength for AZO nanostructures with the different annealing temperature. Figure (6) indicates that the optical conductivity decreases with the increasing the wavelength and the value of optical conductivity about  $10^{13}$  for all annealing samples, this shows the optical response of the material that led to be the movement of electrons through the material and in Figure (7) the electrical conductivity increases with the increasing wavelength for all curves with the value of electrical conductivity at up to  $(10^{11} \text{ S/cm})$ , as wavelength increases, the optical and electrical conductivities take on distinct images, with the optical conductivity being higher than the electrical about 100 (one hundred times).

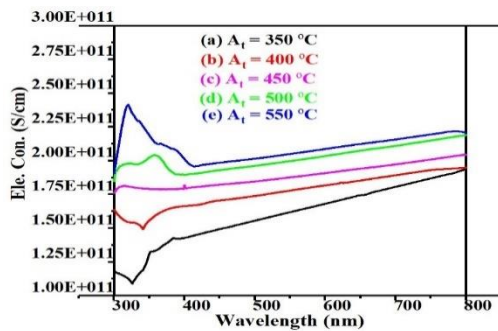


**Figure 7 shows the electrical conductivity for various annealing temperatures: 350, 400, 450, 500, and 550 degrees Celsius.**

In the low wavelength and under (400 nm) at the UV- region exactly, the electrical conductivity various with increasing wavelength and then from decrease then increase until it reaches the visible light region, it continues to rise relatively in this range between 400 and 800 nm.

The electrical conductivity increases for the first two samples, which were annealed at 350 and 400 °C, and appears at a steady state for the sample at 450 °C, in the low wavelength zone, and slowly gradually noticeable with increasing wavelength, the last two samples have a completely different behavior pattern from the behavior pattern of the first two samples, starting with an increase in electrical conductivity in the ultraviolet region (<400 ) nm and then a gradual decrease in the visible spectrum region (> 400) nm until they stabilize and parallel the rest of the other curves with an increase in wavelength (425-800) nm.

The increase of trend in  $\sigma_{ele.}$  upon increase thickness can be attributed to the improvement in the structure of the film as the annealing temperature rises. The results of this study are similar to the results of the research study in terms of behavior [25].

**3.7. The Optical Transmittance:**

Figure 6 displays the optical transmittance spectra of AZO nanostructures that were annealed at various temperatures and fall within the wavelength range of 300–800 nm.

For all samples as shown in Figure 8, the films' optical

transmittance was significantly enhanced by the rising annealing temperature. The AZO films were formed with an average optical transmittance of 73% and 92%, respectively, at annealing temperatures of 500 and 550 °C. The better-formed crystallite that resulted from raising the annealing temperature is what causes the increased optical transmittance. This image shows that transmittance spectra have a sharp edge at a wavelength that corresponds to the quantum energy gap of AZO thin films.

The average transmission values in the visible region were fixed from (425-800) nm and the curve formation seems depending on the annealing temperature. Our results were completely consistent with the researcher's results [19].

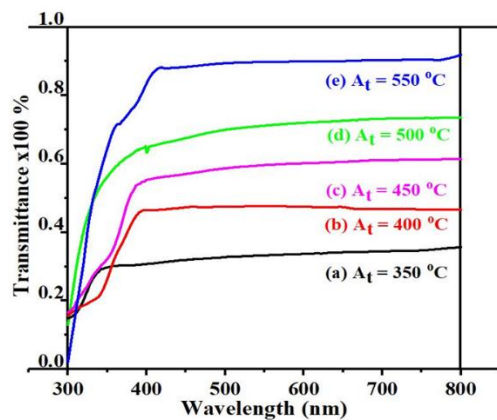


Figure 8, the optical transmittance is shown against wavelength for a range of temperatures used for annealing, such as 350, 400, 450, 500, and 550 °C

### 3.7 The Refractive Index:

The refractive index [26] of the AZO nanostructure samples was calculated from equation (7):

$$n = \frac{\sqrt{1+R}}{\sqrt{1-R}} \dots\dots\dots(7)$$

where R is the reflectance.

Figure 9 shows the samples' refractive indices after being annealed at various temperatures. All samples show that the refractive index of AZO nanostructures on glass substrates reaches its maximum value in the UV region as the annealing temperature increases. Additionally, a short tail, or decrease in refractive index, was observed as the wavelength decreases, which is caused by the electrical transition between bands in photons whose energy is less than the minimum band gap [27] just in two samples which were annealed with (450 & 500) °C. The refractive index increases non-uniformly with the non-uniformly pattern increasing from (350–550) °C, annealed samples due to the improved crystalline structure.

For all samples, and Refractive index is found to decrease with increasing wavelength. Refractive indices decrease rapidly with increased wavelength at between 300 and 400 nm, as well as inside the visible spectrum above the (400 nm) refractive indices record the average value, while the minimum values are achieved at (800) nm.

However, as the temperature of the annealing increases, there is a direct increase in the refractive index's curve. This matches the research [28]. The obtained energy band gap determines how the results vary; as the energy band gap shrank, the refractive index rose [29].

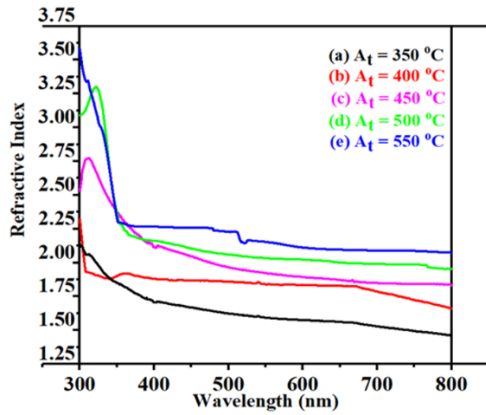


Figure 9, the Refractive Index is plotted against wavelength for various annealing temperatures 350, 400, 450, 500 and 550 °C

### 3.8 Real part and Imaginary part:

The dielectric constant's real part ( $\epsilon_1$ ) and imaginary part ( $\epsilon_2$ ) can be estimated according to the following two equations (8&9):

$$\epsilon_1 = n^2 - k^2 \quad \dots \dots \dots (8)$$

$$\epsilon_2 = 2nk \quad \dots \dots \dots (9)$$

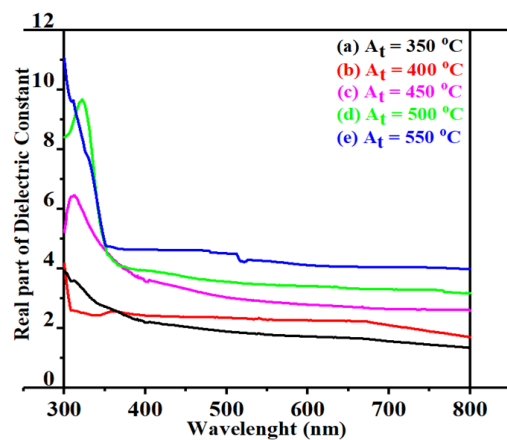


Figure 10: The real component of the dielectric constant for various annealing temperatures as a function of wavelength, (a) 350 °C, (b) 400 °C, (c) 450 °C, (d) 500 °C, and (e) 550 °C

The values of  $\epsilon_1$  and  $\epsilon_2$  for the AZO films at varying annealing temperatures are displayed in Figures 10, 11. The values of  $\epsilon_1$  and  $\epsilon_2$  in the film drop as the wavelength increases. This is indicating their reliance on wavelength. The dielectric constant's

real and imaginary components show the same pattern, with the real part having higher values than the imaginary part. It is evident that in the visible range, the real and imaginary components of the dielectric constant drop with increasing wavelength, whereas in the UV region, they rise.

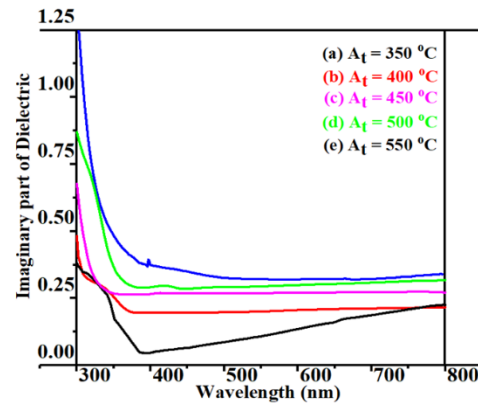


Figure 11 shows the imaginary component of the dielectric constant for various annealing temperatures: 350, 400, 450, 500, and 550 °C

From these two Figures, we can deduce that both the dielectric constant's real and imaginary parts, which behave similarly as they depend on the two equations (8 & 9).

While the imaginary component of the dielectric constant sharply rises in the UV region as the annealing temperature increases, but they are low value in the VIS–NIR area, the real part increases slowly with wavelength decreases at the UV–VIS region and increases in the NIR region. Our results were in line with the researcher's findings, which show that the variance of  $\epsilon_1$  mostly depends on  $n^2$  due to small values of  $k^2$ , whereas  $\epsilon_2$  primarily depends on  $k$  values connected to the absorption coefficient [31].

It can be noticed that the value of  $\epsilon_1$  is significantly greater than  $\epsilon_2$ , and this comparative outcome illustrates

how  $\epsilon_1$  depends on  $n$  when  $n > k$ . As the annealing temperature rises, the actual part of the dielectric constant gradually improves. Conversely, the imaginary part of the dielectric constant falls off rapidly and becomes fixed after 400 nm, whereas it is almost constant in the lower wavelength area.

When examining the structure and flaws in materials, as well as within the sample, the dielectric loss factor ( $\tan(\delta)$ ) is an important tool since it shows the phase difference caused by energy loss. The real and imaginary parts determine the  $\tan(\delta)$  [15], can be estimated according to the following equations (10):

$$\tan \delta = \frac{\epsilon_2}{\epsilon_1} \dots \dots \dots (10)$$

Figure 12 shows the  $\tan(\delta)$  against wavelength graph. Because of the sudden increase in the absorption coefficient, a nearly constant reliance is shown at shorter wavelengths and a substantial dependence can be seen at wavelengths above 400 nm. The nature and cause of dielectric losses are so interesting. Following that, its value dropped in the high wavelength area. As a result, the dissipation factor demonstrated a considerable reliance on wavelength energy. Z. Hana had previously reported on the dissipation factor's observed behavior [15]. It is important to note that, contrary to expectations, the dielectric loss peaks in the two real and imaginary dielectric sections were not seen to correlate with fluctuations in the input photon energy. The numbers  $k$  and  $n$  will affect on the  $\epsilon_1$  and  $\epsilon_2$  values, i.e., as the annealing temperature is raised, the  $\epsilon_1$  and  $\epsilon_2$  values for the annealed AZO nanoparticles rise. This is because the

average grain size, oxygen vacancies, and carrier concentration rise with the annealing temperature. Our findings supported the researcher's findings [30] but disagreed with them [31].

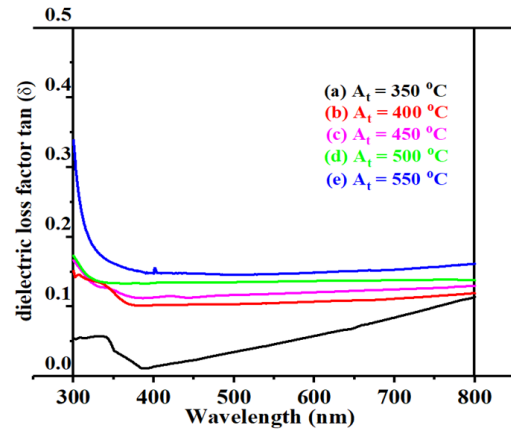


Figure 12 shows the dielectric loss factor for each of the following annealing temperatures: 350 °C, 400 °C, 450 °C, 500 °C, and 550 °C.

#### 4. CONCLUSION

To sum up, we looked at how the annealing temperature affected the optical properties of AZO-NSs that were spin-coated onto a glass substrate following their low-temperature sol-gel production. This study found that the optical properties effected by annealing temperature on the AZO products. The annealed AZO-NSs' UV–Vis absorption spectra showed a small red shift in the absorption peak and a decrease in band gap energy as the annealing temperature rose. This is explained by the fact that crystallite sizes increase at various annealing temperatures. In the visible and IR radiation regions of the spectrum, AZO films at the lower transmittance the annealed at 350 °C, but when the temperature rises to 550 °C, they achieve a higher transmittance of 93%. It was discovered as the annealing temperature was raised, the extinction

coefficient of these AZO films rose. Since they rise in direct proportion to the annealing temperature, it is evident that both optical and electrical conductivity are dependent on the annealing temperature.

### References

- 1- Shakti, N. and Gupta, P.S., 2010. Structural properties & photoluminescence of ZnO thin film and nanowires. *Optoelectronics and Advanced Materials-Rapid Communications*, 4(May 2010), pp.662-664.
- 2- Davydova, M., Gas-sensing behaviour of ZnO/diamond nanostructures. *Beilstein J. Nanotechnol.* 9,(1), 22–29,(2018).
- 3- Jarrah, R.M.S. and Alessa, I.M., 2019. The effect of annealing temperature on the structural and optical properties of nanostructure ZnO. *International Journal of Energy and Environment*, 10(3), pp.163-168.
- 4- Sarma, B.K. and Rajkumar, P., 2020. Al-doped ZnO transparent conducting oxide with appealing electro-optical properties–Realization of indium free transparent conductors from sputtering targets with varying dopant concentrations. *Materials Today Communications*, 23, p.100870.
- 5- Darma, Y., Muhammady, S., Hendri, Y.N., Sustini, E., Widita, R. and Takase, K., 2019. Tuning the point-defect evolution, optical transitions, and absorption edge of zinc oxide film by thermal exposure during molecular beam epitaxy growth. *Materials Science in Semiconductor Processing*, 93, pp.50-58.
- 6- Boughelout, A., Macaluso, R., Crupi, I., Megna, B., Aida, M.S. and Kechouane, M., 2019. Improved Cu<sub>2</sub>O/AZO heterojunction by inserting a thin ZnO interlayer grown by pulsed laser deposition. *Journal of Electronic Materials*, 48, pp.4381-4388.
- 7- Kumar, K.D.A., Mele, P., Ponraj, J.S., Haunsbhavi, K., Varadharajaperumal, S., Alagarasan, D., Algarni, H., Angadi, B., Murahari, P. and Ramesh, K., 2020. Methanol solvent effect on photosensing performance of AZO thin films grown by nebulizer spray pyrolysis. *Semiconductor Science and Technology*, 35(8), p.085013.
- 8- Khan, M.I., Neha, T.R. and Billah, M.M., 2022. UV-irradiated sol-gel spin coated AZO thin films: enhanced optoelectronic properties. *Heliyon*, 8(1).
- 9- Kamaruddin, S.A., Chan, K.Y., Yow, H.K., Zainizan Sahdan, M., Saim, H. and Knipp, D., 2011. Zinc oxide films prepared by sol–gel spin coating technique. *Applied Physics A*, 104, pp.263-268.
- 10- Sengupta, J., Sahoo, R.K., Bardhan, K.K. and Mukherjee, C.D., 2011. Influence of annealing temperature on the structural, topographical and optical properties of sol–gel derived ZnO thin films. *Materials Letters*, 65(17-18), pp.2572-2574.
- 11- Abdelghani, Ghazouan Mahmood, Ali Ben Ahmed, and Aseel Basim Al-Zubaidi. "Synthesis, characterization, and the influence of energy of irradiation on optical properties of ZnO nanostructures." *Scientific Reports* 12.1 (2022): 20016.
- 12- Bekele, B., L. T. Jule, and A. Saka. "The effects of annealing temperature on size, shape, structure and optical properties of synthesized

- zinc oxide nanoparticles by sol-gel methods." *Digest Journal of Nanomaterials & Biostructures* 16.2 (2021): 471-478.
- 13- Mishra, Pooja Nag, Pankaj Kumar Mishra, and Dinesh Pathak. "The influence of Al doping on the optical characteristics of ZnO nanopowders obtained by the low-cost sol-gel method." *Chemistry* 4.4 (2022): 1136-1146.
- 14- Zaka, H., Parditka, B., Erdélyi, Z., Atyia, H.E., Sharma, P. and Fouad, S.S., 2020. Investigation of dispersion parameters, dielectric properties and opto-electrical parameters of ZnO thin film grown by ALD. *Optik*, 203, p.163933.
- 15- Kayani, Z.N., Naz, F., Riaz, S. and Naseem, S., 2017. Characteristics of Al-doped ZnO: Ni films grown on glass by sol-gel dip coating technique. *Journal of Saudi Chemical Society*, 21(4), pp.425-433.
- 16- Goswami, M., Adhikary, N.C. and Bhattacharjee, S., 2018. Effect of annealing temperatures on the structural and optical properties of zinc oxide nanoparticles prepared by chemical precipitation method. *Optik*, 158, pp.1006-1015.
- 17- Alrefae, M., Singh, U.P. and Das, S.K., 2021, August. Growth of ZnO nanostructured thin films by non-conventional sol-gel method and the effect of annealing temperature on its properties. In *Journal of Physics: Conference Series* (Vol. 1973, No. 1, p. 012069). IOP Publishing.
- 18- Ng, Z.N., Chan, K.Y. and Tohsophon, T., 2012. Effects of annealing temperature on ZnO and AZO films prepared by sol-gel technique. *Applied Surface Science*, 258(24), pp.9604-9609.
- 19- Kayani, Zohra N., et al. "Characteristics of Al-doped ZnO: Ni films grown on glass by sol-gel dip coating technique." *Journal of Saudi Chemical Society* 21.4 (2017): 425-433.
- 20- Baydogan, Nilgun, et al. "Refractive index and extinction coefficient of ZnO: Al thin films derived by sol-gel dip coating technique." *Defect and Diffusion Forum*. Vol. 334. Trans Tech Publications Ltd, 2013.
- 21- Mazilu, M., N. Tigau, and V. Musat. "Optical properties of undoped and Al-doped ZnO nanostructures grown from aqueous solution on glass substrate." *Optical Materials* 34.11 (2012): 1833-1838.
- 22- Ahmed, G., Mahmoud, T., Mohammed, H. and Hussein, A., 2021. Fabrication and Study of ZnO thin Films using Thermal Evaporation Technique. *Egyptian Journal of Chemistry*, 64(9), pp.5183-5191.
- 23- Ali, Mohammed J. Mohammed. "Optical and Electrical Conductivity of SnO: Cu Nanoparticles." *Al-Mustansiriyah Journal of Science* 32.3 (2021): 33-41.
- 24- Sedky, A., Atif Mossad Ali, and Mansour Mohamed. "Structural and optical investigation of pure and Al doped ZnO annealed at different temperatures." *Optical and Quantum Electronics* 52 (2020): 1-21.